PAPER • OPEN ACCESS

Cross-correlation-based approach to align turbulent inflow between CFD and lower-fidelity-codes in wind turbine simulations

To cite this article: F Wenz et al 2020 J. Phys.: Conf. Ser. 1618 062005

View the <u>article online</u> for updates and enhancements.



IOP ebooks™

Bringing together innovative digital publishing with leading authors from the global scientific community.

Start exploring the collection-download the first chapter of every title for free.

1618 (2020) 062005

doi:10.1088/1742-6596/1618/6/062005

Cross-correlation-based approach to align turbulent inflow between CFD and lower-fidelity-codes in wind turbine simulations

F Wenz¹, K Boorsma², T Lutz¹ and E Krämer¹

- $^{\rm 1}$ Institute of Aerodynamics and Gas Dynamics, University of Stuttgart, Pfaffenwaldring 21, 70569 Stuttgart, Germany
- 2 Netherlands Organisation for Applied Scientific Research (TNO), Westerduinweg 3, 1755 LE Petten, The Netherlands

E-mail: wenz@iag.uni-stuttgart.de

Abstract. In cases with turbulent inflow, the analysis of the temporal development of forces could provide more insight into differences in calculated fatigue loads of wind turbines. While lifting-line-codes and the Blade-Element-Momentum (BEM) approach do not resolve the inflow, Computational Fluid-Dynamic (CFD) codes resolve the entire flow field. A comparison of time series between the different codes therefore requires a consistent input of the background turbulence. This was enabled by extracting the turbulent velocity field from empty box (without rotor) CFD simulations at the anticipated rotor position. The presence of a rotor in the CFD simulations leads to a delay in the inflow due to the induced velocity. This blockage effect of the rotor was quantified by a cross-correlation. The velocity field extracted from the simulation of the empty box was shifted by the resulting temporal offset before it was used as lifting-line-code or BEM input. Thus, a time-dependent load comparison between the codes could be performed. It was found that the difference in load predictions between CFD and BEM seems to be larger at peak values. For cases with high thrust coefficient or high turbulence intensity, a simpler analytical approach resulted in significantly higher temporal offsets than the cross-correlation.

1. Introduction

Wind energy is one of the most important pillars with regard to the realisation of a sustainable energy supply. Besides opening up new, previously unused areas for wind farms, increasing the size of the wind turbines is a main engineering objective. However, this development is a challenge because tall, skinny blades, operating in higher wind speeds, tend to bend more and the overall loads get higher. High safety factors to account for uncertainties in load prediction, material and manufacturing cause high costs and limit the size of wind turbines. Therefore, it is important to reduce the uncertainty in predicting these loads.

In industry and research, codes with different levels of fidelity are used to calculate the design driving fatigue loads of wind turbines. Within the EU project AVATAR [1] a fatigue load comparison round between various fidelity aero-elastic codes featuring a sweep through the operational regime of a generic 10 MW rotor was performed. Using a vortex wake model, a 15% lower fatigue load was observed compared to the results obtained with the Blade Element Momentum Theory (BEM). When experimental data is not available, high-fidelity Computational Fluid Dynamic (CFD) simulations can be used as numerical reference solutions.

Content from this work may be used under the terms of the Creative Commons Attribution 3.0 licence. Any further distribution of this work must maintain attribution to the author(s) and the title of the work, journal citation and DOI.

1618 (2020) 062005

doi:10.1088/1742-6596/1618/6/062005

In cases with turbulent inflow, the analysis of the temporal development of loads allows, in addition to a statistical evaluation, as described by Ehrich et al. [2], a more detailed investigation of the reasons for the differences between the codes. In BEM and vortex-wake models the flow field including turbulent fluctuations is superimposed directly on the rotor. In CFD simulations, however, the turbulence is injected upstream of the rotor, usually close to the inflow boundary. As a consequence, the turbulent structures are potentially deformed during propagation through the CFD domain [3] and the mean flow velocity upstream of the turbine is slowed down by the rotor blockage [4]. This inconsistency in the input of background turbulence in the different codes prevents a comparison of the resulting load fluctuations based on time series. Therefore, the CFD effects mentioned above must be taken into account to allow for a time-dependent load comparison between the codes.

The aim of the study is to present an approach that allows a time-accurate comparison of the loads calculated with CFD and lifting-line-codes or BEM for turbulent inflow conditions. This may help to better understand the differences between the commonly used BEM-based tools and higher fidelity codes for atmospheric inflow conditions. The functionality is demonstrated with the AVATAR research wind turbine [1]. The simulation approaches and the numerical setup are described in section 2 and section 3, followed by the cross-correlation method in section 4. In section 5 different inflow and operating conditions are evaluated and finally an overview is given in section 6.

2. Simulation methods

This section gives a brief overview of the simulation methods for wind turbines used in this study and the corresponding solvers. The reference solution was calculated with the CFD solver *FLOWer* and the BEM results were obtained with *ECN Aero Module*. The results obtained with lifting-line-codes can be found in [5].

2.1. Computational Fluid Dynamics (CFD)

The most complex, but also most accurate method for calculating the aerodynamics of wind turbines is the CFD simulation, which takes into account the flow around the actual geometry including three-dimensional effects and viscosity. In this study, the CFD simulations are based on the process chain for the simulation of wind turbines, which was developed at the Institute of Aerodynamics and Gas Dynamics (IAG) at University of Stuttgart (e.g. [6]). The basis for the numerical simulations is the CFD solver FLOWer, which is complemented by various preand post-processing tools. FLOWer was developed by the German Aerospace Center (DLR) [7]. It is a compressible, dual time-stepping, block structured Reynolds-averaged Navier-Stokes (RANS) solver. The numerical scheme is based on a finite-volume formulation. The implemented Chimera technique allows the use of independent grids for the individual components of the wind turbine and the background. The solver is continuously extended at the IAG to improve its suitability for wind turbine simulations. Amongst others, the 5th order weighted essentially non-oscillatory scheme WENO is available for spatial discretisation [8] and several RANS and hybrid RANS/LES turbulence models have been implemented in FLOWer to close the Navier-Stokes equation [9]. Furthermore, a body forces approach is included to superimpose atmospheric turbulence on the inflow [10].

2.2. Blade Element Momentum theory (BEM)

BEM is the most commonly used method for calculating the aerodynamics of wind turbines with horizontal axis. Since its computational effort is very low, it is mainly used when many different operating conditions are to be simulated. BEM is an iterative method, which considers individual span-wise sections of the rotor blade independently. It combines momentum theory and blade element theory and enables the calculation of lift and drag forces at the respective blade element

1618 (2020) 062005

doi:10.1088/1742-6596/1618/6/062005

and the associated axial and tangential influence on the flow, based on aerodynamic polars of the blade sections. Many different empirical extensions for the correction of e.g. three-dimensional effects or dynamic stall effects are available. Within this study the ECN Aero Module [11] was used. In order not to average out the effect of inflow fluctuations, i.e. the turbulence, on the local induction, an unsteady BEM formulation is implemented in this BEM tool. In addition, a dynamic inflow model, an oblique inflow model and the Prandtl tip loss correction are available and the turbulent wake state equation is used. Further details are given in [5].

3. Numerical Setup

3.1. Studied wind turbine

The blade geometry of the 10 MW AVATAR research wind turbine [12] is considered in the present study. The radius of the blade is 102.88 m and since only the rotor is simulated without nacelle and tower, the three blades are simply connected in the root region. The rotor was simulated rigidly and no effects resulting from Fluid-Structure-Interaction (FSI) were evaluated.

3.2. CFD model

The CFD model of the AVATAR rotor consists of four independent component meshes embedded in a background mesh by using the Chimera overlapping grid technique, as shown in Figure 1a. In a previous study a blade mesh convergence test was performed [13]. The blade mesh used is a C-type mesh with $[280 \times 128 \times 192]$ grid cells in the chord, wall-normal and span-wise directions. The first wall-off cell size is less than 3×10^{-6} m, which satisfies the condition $y^+ < 1$. A uniform mesh was used as background mesh with a resolution of 1 m to resolve the ambient turbulence [3]. The resolution of 1 m ranges from 448 m upstream to 512 m downstream of the rotor, see Figure 1b. A coarsening of the mesh towards the domain boundaries was applied to reduce the total number of cells. The domain size was set to $[3584 \times 1792 \times 1792]$ m³ in the flow direction (x) and the two lateral directions (y, z). The axis of rotation was aligned with the x-axis and located at the origin (see Figure 1b), which was located at a distance of 1536 m from the inlet boundary. In total, the setup for simulations with the rotor consists of 123.5 million cells.

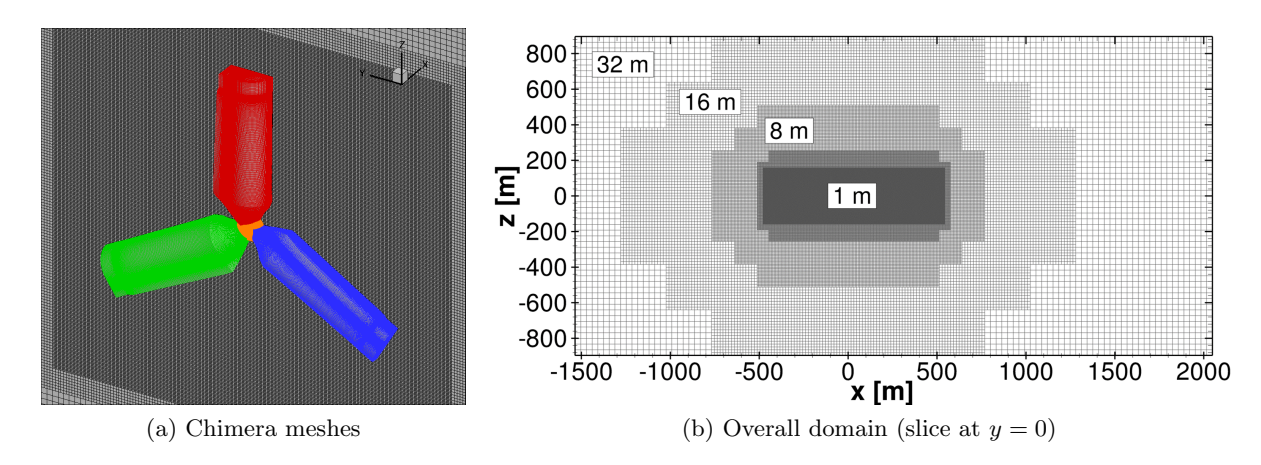


Figure 1: Topology of a) Chimera meshes of blades and connector and b) background mesh.

The Menter SST $k-\omega$ [14] based Improved Delayed Detached Eddy Simulation (IDDES) model [15] was adopted, and no transition model was considered, i.e. fully turbulent simulations were conducted. For the time discretisation a second order dual time stepping method was used and a five-stage Runge-Kutta scheme was applied for every inner-iteration. The second order Jameson-Schmidt-Turkel (JST) scheme [16] was utilized for the blade meshes and the 5th order WENO scheme for the background mesh. On the blade surface, a no-slip wall condition without

1618 (2020) 062005

doi:10.1088/1742-6596/1618/6/062005

any wall function was used and a far-field condition was applied in the cross flow directions, i.e. y, z. A constant velocity and constant pressure were set at the inlet and outlet boundaries, respectively.

The atmospheric turbulence was generated using Mann's model [17] and was injected at $x = -400 \,\mathrm{m}$ using a momentum source term [18], superimposing the steady uniform inflow. In a first wind field, the relevant length scale L was set according to IEC61400-1 [19], in the second a value four times larger than this was used. To comply with the atmospheric conditions according to IEC61400-1, an anisotropic turbulence was generated. As recommended in [20], the stretching factor was chosen as $\Gamma = 3.9$ to approximate the Kaimal spectral model. To achieve the desired turbulence intensity TI in axial direction according to wind turbine class 1A, the turbulence fields were scaled for each mean velocity. In CFD the turbulence is altered as it propagates through the domain [3]. If there is no turbulence generating process such as shear, complex terrain or vegetation, the turbulence decays over time, i.e. with the propagation distance. Besides this physical decay of the turbulence, which also occurs in reality, this process is enhanced by the numerical approach of CFD. The numerical dissipation due to the resolution of the meshes as well as the injection via forces cause a certain turbulence decay within the CFD simulation [3]. Therefore TI at the rotor plane is smaller than the turbulence intensity of the input wind field (TI_{target}) . This effect is taken into account by applying a further scaling factor SF_{CFD} . The factor for this set-up was estimated by running an empty box simulation (without rotor) with a short Mann box (x = 11.9L). The evaluation of the anticipated rotor disk area in the rotor plane and a comparison with the TI of the Mann box resulted in $SF_{CFD} = 1.65$. This agrees well with the results in [3].

In CFD an initialisation simulation is necessary for each case to propagate the turbulence from the injecting position at $x=-400\,\mathrm{m}$ to the rotor position. These simulations were conducted with a constant mean rotor speed ω and a constant pitch angle β . The simulation length of the initialisation was chosen separately for each case to ensure that the turbulence also covers the wake and that the induction effect can develop properly. For the initialisation simulation the time step is $\Delta t \approx 2^{\circ}$ with 45 inner iterations according to the AVATAR baseline setting [21]. After initialisation, the time step was halved to achieve about 1° azimuthal variation of the blades per time step for the main simulation.

3.3. Simulation cases

Within the conducted study, six inflow cases were considered, which are listed in Table 1. The mean inflow velocity u_{∞} , the resulting turbulence intensity at the rotor position TI, the turbulent length scale L and the impact of the controller on the rotational speed ω and the pitch β are varied. A discussion of the values can be found in [5].

Table 1: Inflow and operating conditions as well as resulting thrust coefficient c_t , induction factor a_o , temporal offset at rotor position via cross-correlation $\tau_{0,c}$ and analytical model $\tau_{0,a}$.

Case	$u_{\infty}[\mathrm{m/s}]$	TI[%]	L[m]	$\omega[{ m rpm}]$	β[°]	$c_t[-]$	$a_0[-]$	$ au_{0,a}[\mathbf{s}]$	$ au_{0,c}[\mathbf{s}]$
AVATAR_10.5LOW	10.5	6.4	89.5	9.022	0.0	0.67	0.21	1.0	0.9
$8ms_TI23_fix$	8.0	23.9	33.6	6.874	0.0	0.56	0.17	1.2	0.9
$16 \mathrm{ms}_{ ext{-}} \mathrm{TI17}$	16.0	14.2	33.6	var	var	0.45	0.13	0.5	0.5
$8ms_TI10$	8.0	12.3	33.6	var	0.0	0.55	0.16	1.2	1.4
$8ms_highCt$	8.0	23.9	33.6	var	1.5	0.77	0.26	1.9	1.3
$8 ms_highL$	8.0	27.1	134.4	var	0.0	0.59	0.18	1.7	1.5

1618 (2020) 062005

doi:10.1088/1742-6596/1618/6/062005

4. Methodology

As mentioned above, in CFD the turbulence is altered as it propagates through the domain. In addition, the propagation is slowed down upstream of the turbine due to the rotor blockage. According to the experimental results of Medici et al. [4] a wind turbine affects the flow in a region extending at least three rotor diameters upstream the rotor position. In BEM and vortex-wake models, the flow field, i.e. the turbulence, is injected directly on the rotor and the blockage is accounted for via the induction factor. In order to enable a time-dependent load comparison between the codes, the mentioned effects of CFD must be accounted for in the input of lifting-line-codes and BEM.

The approach to enable a time-accurate comparison between the codes consists of multiple steps. First, the CFD simulation with the rotor is performed using the desired inflow conditions, thus creating the reference solution for the comparison. The second step is to ensure that the flow field hitting the rotor is as similar as possible for all codes. To include the deformation of turbulent structures and the turbulence decay during propagation in CFD in lifting-line-codes or BEM, an empty box (without rotor) CFD simulation is performed using the same structured background mesh that is used in the rotor simulation. From this simulation, the turbulent velocity field is extracted at the intended rotor position to be used as input for lifting-line-codes or BEM. However, in an empty box CFD simulation, the induction of the rotor and the corresponding reduction of the propagation speed (axial flow velocity) is missing. This means that in CFD simulations with consideration of a rotor a certain turbulent vortex reaches the rotor position a little later than in an empty box CFD simulation. Therefore, in a third step this temporal offset $\tau_{0,c}$ is quantified. Finally, the extracted velocity field from the empty box CFD simulation is shifted by the temporal offset $\tau_{0,c}$ before it is used as input to lifting-line-codes or BEM. This procedure provides a velocity input to the rotor in lifting-line-codes and BEM that is almost identical (in space and time) to what the rotor sees in CFD.

The quantification of the necessary temporal offset $\tau_{0,c}$ and the confirmation of the similarity of the flow fields of the two CFD simulations, with and without rotor, is done by means of a cross-correlation approach. The cross-correlation is evaluated at more than 12000 points in several planes perpendicular to the rotor axis upstream of the rotor position at $\xi_n = x_n/R$, where x_n is the upstream position of the plane from the rotor and R is the rotor radius. Input for the cross-correlation is the flow velocity of the CFD simulation with rotor (index rotor) and the flow velocity of the empty box CFD simulation (index empty). The normalized cross-correlation (NCCF) C_{ii} for the velocity component i between the two cases is

$$C_{ii}(\xi_n, y, z, \tau_c) = \frac{\sum_{t=t_0}^{T} u'_{empty,i}(\xi_n, y, z, t) \cdot u'_{rotor,i}(\xi_n, y, z, t + \tau_c)}{\sqrt{\sum_{t=t_0}^{T} \left(u'_{empty,i}(\xi_n, y, z, t)\right)^2 \cdot \sum_{t=t_0}^{T} \left(u'_{rotor,i}(\xi_n, y, z, t + \tau_c)\right)^2}}$$
(1)

The value C_{ii} is a measure for the similarity between the two velocity fluctuation u_i' time series at a certain position (ξ_n, y, z) in space. The length of the compared time series $T - t_0$ is chosen as long as available, where t_0 is the time after which the wake is sufficiently developed and the turbulence is propagated beyond the turbine in the CFD simulation. This approach makes it possible to determine to what extend the rotor has altered the turbulence characteristic, respectively the velocity time series. Moreover, the blockage effect can be quantified per plane in the form of a temporal offset by determining τ_c , which gives the maximum C_{ii} . The locally varying temporal offset for each velocity component (u, v, w) is then averaged over the rotor-disk-area in each plane before the three resulting $\tau_{c,ii}$ values per plane are also averaged. Finally, the single values per plane are used to extrapolate the temporal offset $\tau_{0,c}$ at the rotor plane by performing a least-square-fit with $\tau(\xi) = a \cdot exp(b \cdot \xi)$. Using an exponential trend resulted in the least deviation at the data points.

1618 (2020) 062005

doi:10.1088/1742-6596/1618/6/062005

5. Results

5.1. Pre-study with AVATAR case

The described workflow was developed and tested with the already existing AVATAR case 10.5LOW [21], as summarised in Table 1.

Looking at a segment of the axial velocity component time series of the CFD simulation with and without rotor at $\xi = -0.5$, y = 0 and z = 0 in Figure 2a, the three expected phenomena are visible. Firstly, the course of the velocity is quite similar. Secondly, the axial velocity is reduced in the simulation with rotor and finally there is a small temporal offset between the time series. The main focus is on the temporal offset quantified with the cross-correlation $(T - t_0 \approx 100 \,\mathrm{s})$. Figures 2b and 2c show the spatial y-z-distributions of the best temporal offset in two planes. As expected, the offset increases with decreasing distance to the rotor plane. In the presented method (section 4), the local temporal offsets are averaged over the rotor disk area in each y-z-plane to obtain a single value per ξ_n . However, especially near the rotor $(\xi = -0.5)$ in Figure 2c, a larger offset τ_c occurs in the root area than in the tip region of the blades.

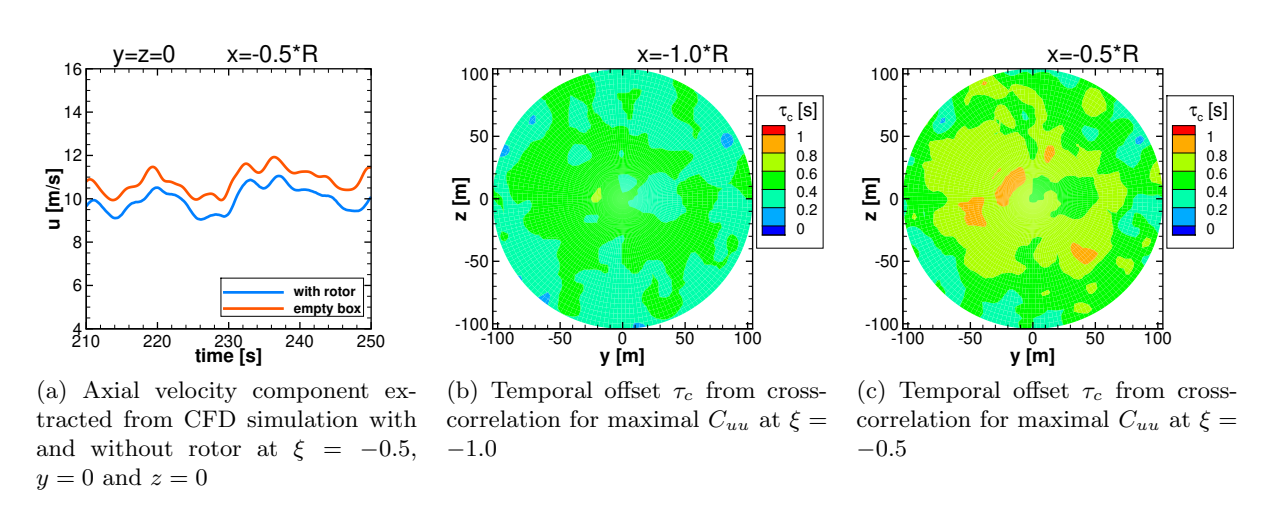


Figure 2: Velocity time series and spatial distribution of temporal offset τ_c for turbulent inflow alignment of AVATAR case 10.5LOW.

Therefore, the temporal offset τ_c of the cross-correlation at $\xi = -0.5$ was only averaged over the azimuth and over the three velocity components in order to keep a radial dependency. Figure 3a shows the resulting radial distribution. This radius-dependent temporal offset was applied to the velocity field of the CFD simulation with rotor before the cross-correlation was recalculated. The distribution of the resulting cross-correlation values C_{uu} in Figure 3b is very similar to the one with constant temporal offset depicted in Figure 3c. Hence, it was decided that the benefit of the radius-dependent compensation of the rotor blockage is negligible for the AVATAR rotor, which features a more or less constant induction with span.

Overall, the similarity of the velocity fields between the empty box CFD simulation and the CFD simulation with rotor near ($\xi = -0.5$) the rotor position is quite high over the whole rotor disk area when the quantified temporal offset τ_c is applied (see Figure 3c). Hence, the turbulent wind fields of the simulation with and without rotor were found to be reasonably well aligned. This justifies the assumption that the overall turbulence characteristics of the inflow are not significantly altered by the induction of the rotor when approaching the rotor position, except in the near-field for $\xi \to 0$. Therefore, the velocity field extracted from the empty box simulation at $\xi = 0$ could be used as input for lifting-line-codes or BEM. To allow time-dependent comparisons of the loads to CFD, the extracted velocity field must be shifted by the extrapolated $\tau_{0,c}$ before it can be used in lifting-line-codes or BEM.

1618 (2020) 062005

doi:10.1088/1742-6596/1618/6/062005

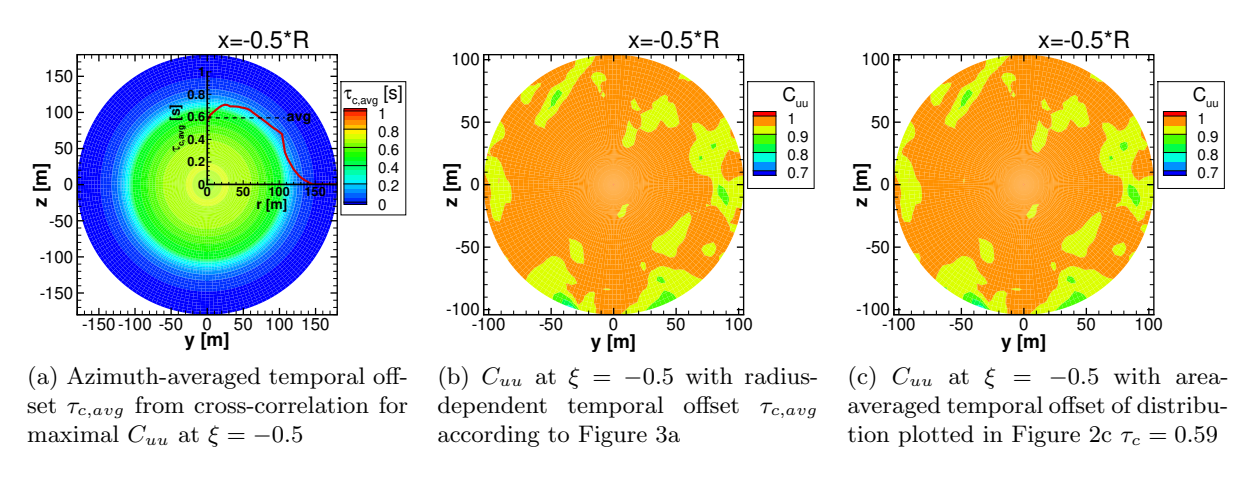


Figure 3: Radius-dependent temporal offset and spatial distribution of axial cross-correlation value C_{uu} for turbulent inflow alignment of AVATAR case 10.5LOW.

5.2. Quantification of temporal offset

The quantification of the temporal offset $\tau_{0,c}$ between the CFD simulation with and without rotor is shown in more detailed for the case 8ms_TI23_fix. Figure 4a shows a segment of the axial velocity component time series of the CFD simulations with and without rotor at $\xi = -2.0$, y = 0 and z = 0. The time series are almost identical, which allows the conclusion that the induction zone barely reaches $\xi = -2.0$. This is less than in [4] and [22] for steady wind conditions and similar c_t . However, turbulence causes the wake to break down faster, which also reduces the induction zone upstream. Figure 4b depicts the velocity time series at $\xi = -0.5$. The same phenomena as described in the previous section occur, but the higher TI is visible.

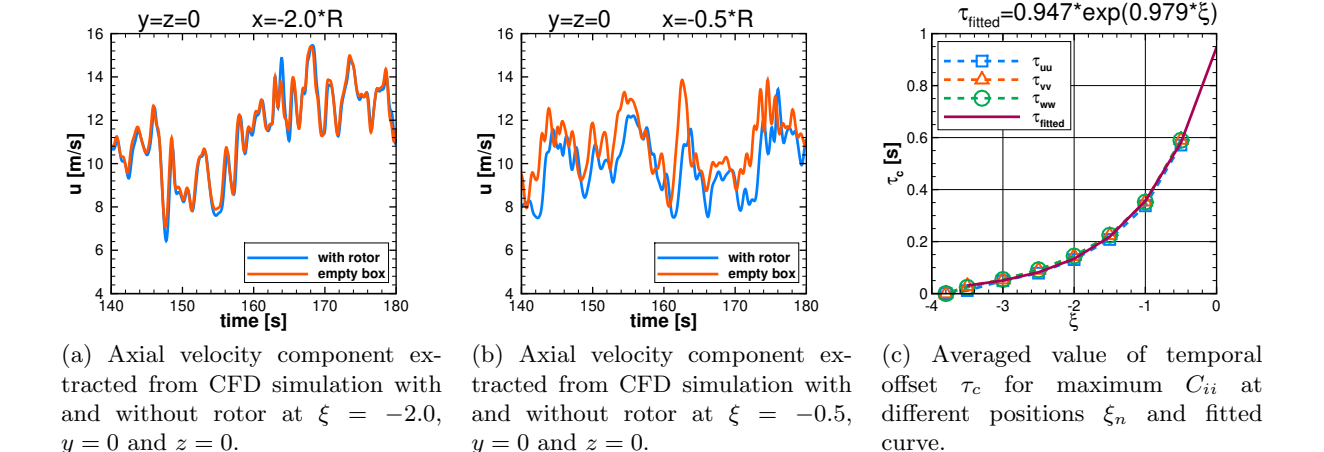


Figure 4: Velocity time series and cross-correlation results of case 8ms_TI23_fix.

The averaged temporal offset τ_c for each velocity component in each plane obtained with the cross-correlation $(T-t_0\approx 134\,\mathrm{s})$ is shown in Figure 4c against ξ . The three velocity components give very similar progressions of τ_c and, as expected, the temporal offset increases with decreasing distance from the rotor. The fitted exponential curve matches well and results in a temporal offset $\tau_{0,c}=0.95\,\mathrm{s}$ at the rotor position (see Table 1 for all cases). This means that the extracted velocity field from the empty box CFD simulation must be shifted by this value before it can be used as input in lifting-line-codes or BEM.

1618 (2020) 062005

doi:10.1088/1742-6596/1618/6/062005

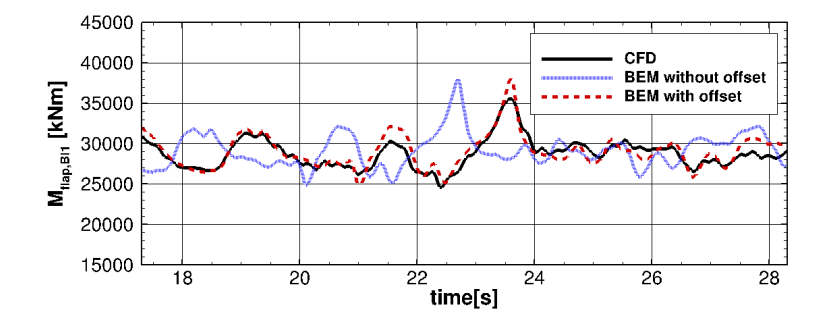


Figure 5: Comparison of the flapwise blade root moment M_{flap} between CFD and BEM with and without taking the time offset into account.

Figure 5 shows exemplarily the time series of M_{flap} of one blade from the CFD simulation as well as from BEM with and without consideration of the temporal offset. The curve resulting from BEM fits the CFD result very well when the temporal offset is taken into account. It can be seen that BEM seems to overestimate load peaks, while the mean value is quite similar to the CFD results. This confirms the previously observed differences in fatigue loads [5].

5.3. Comparison to analytical model

The results for the temporal offset obtained with the cross-correlation from the CFD results (τ_c) were compared with an analytical estimation of the time offset based on the axial induction factor at the rotor plane $a_0 = (u_\infty - u_0 (\xi = 0)) / u_\infty$, respectively the thrust coefficient c_t , which can also be obtained directly from BEM. This is done by means of the analytical equation derived by Medici et al. [4]. Using the Biot-Savart law on the vortex sheet theory, they derived an expression for the velocity $u(\xi)$ upstream of the wind turbine at the center line of the rotor for uniform inflow. According to the averaging over the rotor disk in the cross-correlation method, the empirical scaling function $f(r,\xi)$ found by Troldborg and Meyer Forsting [22], which takes into account the decreasing influence of the blockage towards the tip of the blade, is averaged over the rotor disk area

$$\overline{f(\xi)} = \frac{1}{\pi} \int_0^{2\pi} \int_0^1 f(\tilde{r}, \xi) \cdot \tilde{r} \, d\tilde{r} d\varphi = 2 \cdot \int_0^1 \left(\frac{1}{\cosh\left(\beta \frac{\tilde{r}}{\sqrt{\lambda \cdot (\eta + \xi^2)}}\right)} \right)^{\alpha} \cdot \tilde{r} \, d\tilde{r} \quad \text{with } \tilde{r} = \frac{r}{R} \,, \quad (2)$$

and multiplied with the induced velocity at the center line. The coefficients were determined empirically [22] to $\alpha = \frac{8}{9}$, $\beta = \sqrt{2}$, $\lambda = 0.587$ and $\eta = 1.32$. The mean temporal offset over the rotor disk τ_a due to the rotor blockage calculated with the induction factor a_0 can be approximated by integrating the reciprocal of the velocity along the axial distance and subtracting the time required for undisturbed flow

$$\tau_{a} = \left(\frac{R}{u_{\infty}} \int_{-6}^{\xi_{n}} \frac{1}{1 - a_{0} \left[1 + \frac{\xi}{\sqrt{1 + \xi^{2}}}\right] \cdot \overline{f(\xi)}} d\xi\right) - \frac{R \cdot (\xi_{n} + 6)}{u_{\infty}} \quad \text{with } a_{o} = \frac{1}{2} - \frac{1}{2} \cdot \sqrt{1 - c_{t}} . \quad (3)$$

The lower limit is set to $\xi = -6$, assuming that further away from the rotor the blockage effect has no impact on the flow. The upper limit is equal to the position of the planes ξ_n . The derived analytical equation is only valid for $\xi < -1$ [22]. The thrust coefficient from CFD is calculated with $c_t = F_x/(0.5\rho Au_\infty^2)$.

1618 (2020) 062005

doi:10.1088/1742-6596/1618/6/062005

Table 1 gives the thrust coefficients from CFD calculated with the mean thrust F_x and the mean inflow velocity u_{∞} in the rotor disk area in the time interval which is used for the cross-correlation. The corresponding induction factors are also listed. Since the analytical equation is only valid for $\xi < -1$, the temporal offset at $\xi = 0$ is extrapolated using a least-square-fit to an exponential equation, too. The resulting temporal offsets $\tau_{0,a}$ are given in Table 1.

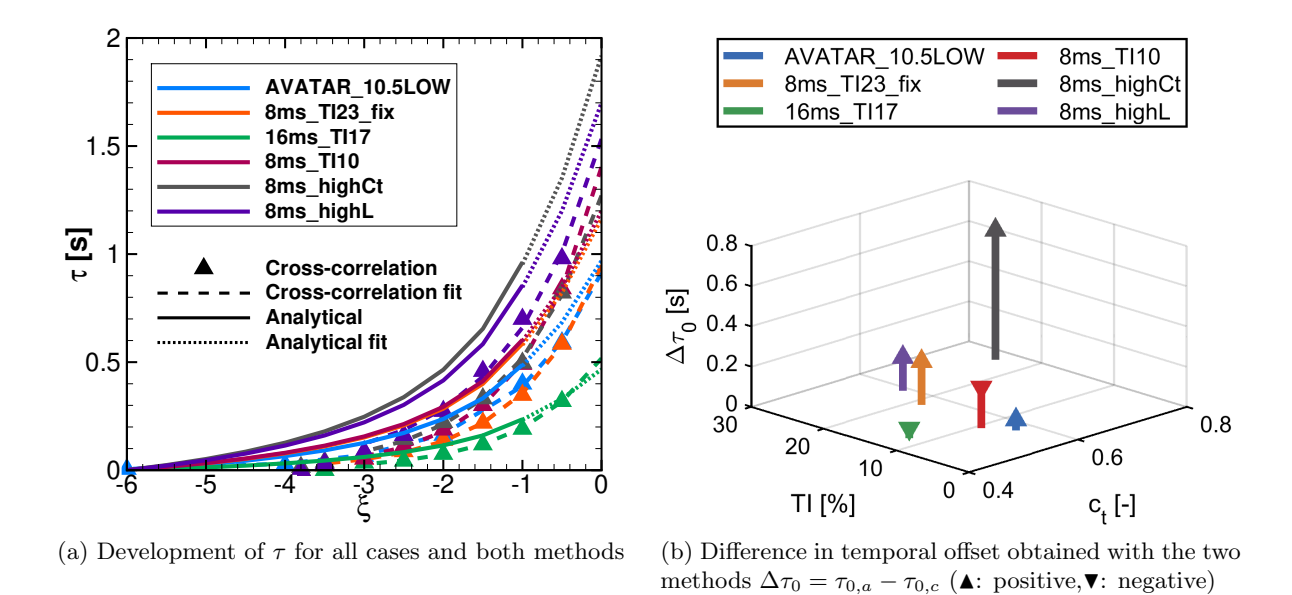


Figure 6: Temporal offset a) against ξ and b) difference of τ_0 against c_t and TI.

Figure 6a shows the development of the temporal offset in the turbulent inflow obtained with the cross-correlation $(T-t_0>57\,\mathrm{s}$ for all cases) as well as the analytical expression. The extrapolated curves are also plotted. Overall, the trend is similar between the two methods, but the differences in the extrapolated temporal offset in the rotor plane are fairly large for some cases. Figure 6b shows $\Delta \tau_0 = \tau_{0,a} - \tau_{0,c}$ against c_t and TI. For cases with high thrust coefficient and high turbulence intensity the differences are bigger. Since the analytical equation is based on strong simplifications such as the actuator disk and constant thrust, which is not given in this study, some differences were to be expected. Moreover, high turbulence intensity makes the exact definition of u_{∞} more difficult and leads to a faster collapse of the wake and thus to a reduction of the blockage. This is partially consistent with the finding in [23], where it was shown that the influence of TI on the induced velocity increases with higher turbulence intensity even below 15%, allowing the assumption that the effect is much stronger for TI > 15%.

6. Conclusions

The development of the turbulence in a domain with and without rotor was analysed with scale-resolving CFD simulations. It could be shown that the turbulent structures change only slightly when approaching the rotor and that the time delay τ_0 caused by the blockage of the rotor can be quantified with a cross-correlation of the velocity fields if the rotor has a fairly uniform induction distribution. Thus, a time-dependent load comparison between lifting-line-codes or BEM and CFD can be performed if a velocity field extracted from an empty box CFD simulation at $\xi = 0$ and shifted by τ_0 is used as input. With this approach it was found that BEM overpredicts the peaks of the aerodynamic loads. A simpler, analytical approach showed the same trend for τ_0 , but differs significantly in absolute value for cases with high thrust coefficient or high turbulence intensity.

1618 (2020) 062005

doi:10.1088/1742-6596/1618/6/062005

Acknowledgments

The studies were conducted within the joint TKI WoZ research project VortexLoads [24], which was carried out with Topsector Energie subsidies from the Dutch Ministry of Economic Affairs. The authors gratefully acknowledge the High-Performance Computing Center Stuttgart (HLRS) for providing computational resources within the project WEALoads. The paper is based on the work of Yusik Kim.

References

- [1] Schepers J et al. 2018 Final results from the EU project AVATAR: Aerodynamic modelling of 10 MW wind turbines Journal of Physics: Conference Series 1037 022013
- [2] Ehrich S, Schwarz C, Rahimi H, Stoevesandt B and Peinke J 2018 Comparison of the blade element momentum theory with computational fluid dynamics for wind turbine simulations in turbulent inflow Applied Sciences 8 2513
- [3] Kim Y, Weihing P, Schulz C and Lutz T 2016 Do turbulence models deteriorate solutions using a non-oscillatory scheme? *Journal of Wind Engineering and Industrial Aerodynamics* **156** 41–49
- [4] Medici D, Ivanell S, Dahlberg J and Alfredsson P 2011 The upstream flow of a wind turbine: blockage effect Wind Energy ${\bf 14}$ 691–697
- [5] Boorsma K, Aman M, Lindenburg C and Wenz F 2019 Validation of BEM and vortex-wake models with numerical tunnel data, TKI WoZ Vortexloads WP2. technical report TNO R11389 http://publications.tno.nl/publication/34634924/jVkOuF/TNO-2019-R11389.pdf
- [6] Klein L, Gude J, Wenz F, Lutz T and Krämer E 2018 Advanced computational fluid dynamics (CFD)—multi-body simulation (MBS) coupling to assess low-frequency emissions from wind turbines Wind Energy Science 3 713–728
- [7] Kroll N, Rossow C, Becker K and Thiele F 2000 The MEGAFLOW project Aerospace Science and Technology 4 223–237
- [8] Kowarsch U, Keßler M and Krämer E 2013 High order CFD-simulation of the rotor-fuselage interaction 39th European Rotorcraft Forum, Moscow
- [9] Weihing P, Letzgus J, Bangga G, Lutz T and Krämer E 2018 Hybrid RANS/LES capabilities of the flow solver flower application to flow around wind turbines *Progress in Hybrid RANS-LES Modelling* (Springer International Publishing) pp 369–380
- [10] Schulz C, Klein L, Weihing P and Lutz T 2016 Investigations into the interaction of a wind turbine with atmospheric turbulence in complex terrain *Journal of Physics: Conference Series* **753** 032016
- [11] Boorsma K, Grasso F and Holierhoek J 2011 Enhanced approach for simulation of rotor aerodynamic loads EWEA Offshore Conference (Amsterdam)
- [12] Sieros G et al. 2015 AVATAR reference blade design, AVATAR deliverable 1.2 https://www.eera-avatar.eu/publications-results-and-links/
- [13] Bangga G, Lutz T, Jost E and Krämer E 2017 CFD studies on rotational augmentation at the inboard sections of a 10 MW wind turbine rotor *Journal of Renewable and Sustainable Energy* 9 023304
- [14] Menter F 1994 Two-equation eddy-viscosity turbulence models for engineering applications AIAA journal 32 1598–1605
- [15] Shur M, Spalart P, Strelets M and Travin A 2008 A hybrid RANS-LES approach with delayed-DES and wall-modelled LES capabilities International Journal of Heat and Fluid Flow 29 1638–1649
- [16] Jameson A, Schmidt W and Turkel E 1981 Numerical solution of the euler equations by finite volume methods using runge kutta time stepping schemes 14th fluid and plasma dynamics conference
- [17] Mann J 1994 The spatial structure of neutral atmospheric surface-layer turbulence *Journal of fluid mechanics* 273 141–168
- [18] Troldborg N, Sørensen J, Mikkelsen R and Sørensen N 2014 A simple atmospheric boundary layer model applied to large eddy simulations of wind turbine wakes Wind Energy 17 657–669
- [19] International Electrotechnical Commission et al. 2005 IEC 61400-1: Wind turbines part 1: Design requirements International Electrotechnical Commission 54–56
- [20] Larsen T and Hansen A 2015 How 2 HAWC2, the user's manual 69
- [21] Kim Y et al. 2016 AVATAR Deliverable D2.5: Effects of inflow turbulence on large wind turbines http://www.eera-avatar.eu/fileadmin/avatar/user/avatar_D2p5_revised_20161231.pdf
- [22] Troldborg N and Meyer Forsting A 2017 A simple model of the wind turbine induction zone derived from numerical simulations Wind Energy 20 2011–2020
- [23] Meyer Forsting A 2017 Modelling Wind Turbine Inflow: The Induction Zone Ph.D. thesis DTU Wind Energy
- [24] Boorsma K, Wenz F, Aman M, Lindenburg C and Kloosterman M 2019 TKI WoZ VortexLoads final report. technical report http://publications.tno.nl/publication/34634923/tbIASC/TNO-2019-R11388.pdf